



# Additive manufacturing of biomorphic scaffolds for bone tissue engineering

Fabrizia Caiazzo<sup>1</sup> · Vittorio Alfieri<sup>1</sup> · Brahim David Bujazha<sup>1</sup>

Received: 31 August 2020 / Accepted: 3 February 2021 / Published online: 26 February 2021  
© The Author(s) 2021

## Abstract

Bone tissue engineering has evolved owing to new opportunities of deep customisation offered by additive manufacturing technologies. Gyroid structures, which have been widely used for energy absorption or chemical catalysis, are now being employed as biomorphic structures as well to provide customer-oriented scaffolds for missing or injured bones. Unfortunately, limited data in terms of manufacturability and mechanical properties are available in the literature to support a wide application scope, because the bone to match is strongly dependent on the individual. Therefore, the study aimed at addressing this lack of knowledge, assessing the manufacturability of metal gyroids and further developing the correlation of the structural response with the designed geometry, so to allow the designer to provide the proper biomorphic structure on a case-by-case basis. Biocompatible steel was used to manufacture samples via laser powder-bed fusion; their elastic moduli and yield strengths were evaluated as a function of the orientation of the elementary cells, the symmetry and the wall thickness based on compression testing. Grounds have been given to support potential applications for tibias and vertebrae.

**Keywords** Additive manufacturing · Gyroids · Bone tissue engineering · Laser powder-bed fusion · Bone scaffold

## 1 Introduction

Many techniques have been reported in the literature for replacing missing or injured bones; these include surgery, drug therapy and artificial prostheses. However, they may cause severe pain, infections or immune rejection [1]. Additionally, bone structures may significantly vary depending on age, gender, health conditions, nutrition and location in the body [2–4]. To this end, bone tissue engineering (BTE) has been recently developed as a multidisciplinary field aiming at inducing bone regeneration using biomaterials, cells and factor therapy [5]. Since the variation range of the bone properties is

significantly wide, the main focus of the research in this field is the selection of a proper method allowing to conveniently mimic the mechanical response, depending on the individual requirements.

Scaffolds are conveniently designed and implanted as an artificial biocompatible extracellular matrix to mimic a natural microenvironment; hence, tissue regeneration is enabled through live cells of bones [1, 6]. The main features of an ideal scaffold in bone and cartilage engineering were pointed out in a prior study [7]. Both *in vitro* and *in vivo* studies were also reported [8, 9].

A macroscale void fraction (e.g. in the form of interconnected porosity with 100- $\mu\text{m}$  diameter [9] at least) is crucial for promoting the adhesion and mass transport of nutrients over the scaffold and achieving both osteoconductivity and osteoinductivity [10]. Data from *in vivo* tests revealed that the ideal pore size for bone substitutes ranges from 0.7 to 1.2 mm [11]. Unfortunately, conflicting requirements of topological features must be addressed, given that porosity is detrimental to the purpose of mechanical stiffness, fatigue life [9] and energy absorption [12].

A wide range of new opportunities in BTE has been offered by the recent advances in the field of additive manufacturing (AM). In particular, processing of ceramics, polymers and

---

✉ Vittorio Alfieri  
valfieri@unisa.it

Fabrizia Caiazzo  
f.caiazzo@unisa.it

Brahim David Bujazha  
brahimdbuj@gmail.com

<sup>1</sup> Department of Industrial Engineering, University of Salerno, Via Giovanni Paolo II 132, 84084 Fisciano, Italy

metals constitutes a new branch of computer-aided BTE [10]. Complex geometries, such as lightweight lattice structures for biomedical applications [13] and even pieces for automotive [14] and aerospace [15, 16], were addressed via AM through layer-by-layer fabrication. Although many AM techniques have been reported in the literature [17, 18], powder-bed fusion using laser [4, 19, 20] or electron beam [21, 22] is assumed to enable the manufacture of metal biocompatible scaffolds with suitable mechanical properties and accuracy for BTE and orthopaedic implants in general, as reviewed in the literature [23].

Owing to AM, the control over the final mechanical and biological features of scaffolds is enhanced at the design stage. Custom-oriented structures can be effectively produced to match the individual requirements. Indeed, convenient geometry and fraction of voids enable the reduction of the metal strength, aiming at matching the properties of bones on a case-by-case basis. Functionally graded pieces can be even manufactured by proper design of the architecture and the void distribution along the scaffold [24]; namely, the size distribution of the pores is given a direction, so to benefit from a specific variation of properties [25]. This is crucial in reproducing the actual structure of a natural bone, wherein the outer part (i.e. the cortical bone) has a higher mechanical strength and modulus in comparison with those of the inner part (i.e. the cancellous or trabecular bone, resembling sponge or foam materials with lower strength) [9]. Moreover, it has been shown that the levels of the governing factors of the building technique can be adequately set to achieve additional microscale porosity [26], further promoting the process of bone ingrowth [27]. Although the trabecular bone accounts only for approximately 20% of the overall bone structure, it is responsible for approximately 70% of bone remodelling [5]. Therefore, it represents the focus of many research activities.

Many arrangements have been proposed and investigated, including basic cube or triangular prism, up to rhombic dodecahedrons and the algorithm to generate them has been explored [28]. Nevertheless, to reproduce adequately the trabecular bone, AM-made scaffolds with an excellent combination of mechanical and mass transport properties were suggested in the form of triply periodical minimal surfaces (TPMSs) [20]. These are 3D surfaces with zero mean curvature that exhibit translational symmetries in three independent directions. Owing to their high stiffness, TPMSs have been considered in many applications [29], including absorption of energy and chemical catalysis. Interestingly, they exhibit biomorphic features as they approach the mean curvature of a trabecular bone, which is close to zero [30, 31]. Among the possible TPMSs, a gyroid lattice is a 3D continuous surface, first proposed by Alan Schoen in the 70s, containing no planar symmetry nor straight lines, offering a structural response depending on

its topology; therefore, many design parameters are effectively offered to accommodate the mechanical response in such a wide range for BTE [32]. Namely, gyroids are formed by consecutively arranging some elementary units and are significantly interesting owing to a remarkable resemblance with the trabecular bone because the biomorphic design and surface-to-volume ratio are enhanced, thereby improving cell adhesion [19, 33] and accessibility of fluid, compared to hexagonal structures [34]. Isotropic elasticity is even offered [35].

Different authors agree [4, 24, 29] that the commercial application of TPMSs and gyroids for BTE is limited to specific cases owing to the reduced amount of data available in the literature on the correlation of the structural response with the manufacturability and the designed geometry, although there is agreement in the last decade on the effectiveness of AM, specifically laser powder-bed fusion, to the scope [36]. More specifically, it is expected that nano- and micro-technology combined with AM may significantly improve the accuracy of AM-derived bone scaffolds [37].

At first, the manufacturability strongly depends on the available powder and the machine; therefore, transferability is limited. For example, it has been shown that the thickness of a steel scaffold may be up to 40  $\mu\text{m}$  thicker than the designed size [19], resulting in a 13% relative error with the nominal thickness. The issue has been investigated for titanium diamond-type cellular lattice [38] and gyroids [39] as well, showing a relative error in the strut thickness up to 20% on average.

As regarding the correlation of the mechanical response with the designed geometry, some authors approached the study, but they focused on the investigation of only some geometric factors, depending on the application. At first, the effectiveness of the gyroids over other structures has been shown, under same volume fractions [40]. More specifically, the elastic modulus and the compressive yield stress have been measured for a given gyroid geometry with three different levels of the void fraction to show that the toughness of the scaffold is increased when the volume fraction increases [19]. The response of several steel gyroids was related to their orientation via analytical and finite element solutions; however, only a given loading direction with a given volume fraction was experimentally tested to verify the reliability of the simulation [4]. A wider study was conducted on titanium gyroids to correlate the geometry to the resulting stiffness, although limited experimental results were reported [29]. The fatigue life of functionally graded parts was investigated as well [24], but only three types of structures were proposed; therefore the results are not extensive to accommodate the actual significant variation of the bone properties.

Parallel efforts were made to match the expected requirements successfully in terms of topology, strength and even permeability of titanium gyroid lattices [20]; however, the

effect of the design parameters was not addressed given that the study aimed at comparing different TPMSs. Nevertheless, two different experimental setups using electron beam melting and the same titanium alloy [21, 22] proved that the wavelength of the gyroid severely affects the mechanical response, leading to accentuated anisotropy and limitations of implantation applicability.

To contribute to the current knowledge in the field, steel gyroids were designed, manufactured via powder-bed fusion and tested in this study to investigate the dependence of the resulting mechanical properties on design parameters, such as orientation, wavelength and thickness. At first, the accuracy has been checked; then, the elastic modulus and the yield strength, which are among the main features to match when designing a biomorphic scaffold, have been measured. With this approach, the authors aim at assessing the manufacturability of metal gyroids via AM and determining a correlation to design custom-oriented TPMSs properly.

## 2 Material and methods

### 2.1 Design of gyroids

As reported in the literature [29], the primary design parameter of an elementary gyroid unit is the wavelength or unit cell size, which can be independently set for each axis. For a given reference size  $L$ , the length  $L_i$  along each axis is conveniently expressed using the corresponding scale factor  $k_i$  accounting for the geometric expansion:

$$L_i = k_i L$$

Under these conditions, the equation of a 3D gyroid lattice surface  $G$  in an  $xyz$  reference system is as follows:

$$G = \sin\left(\frac{2\pi x}{L_x}\right) \cos\left(\frac{2\pi y}{L_y}\right) + \sin\left(\frac{2\pi y}{L_y}\right) \cos\left(\frac{2\pi z}{L_z}\right) + \sin\left(\frac{2\pi z}{L_z}\right) \cos\left(\frac{2\pi x}{L_x}\right)$$

Two additional factors are required: the orientation  $\alpha$ , to arrange the elementary units with respect to each axis, and the wall thickness  $T$ , to upgrade the 3D surface to a finite volume (Fig. 1). Therefore, the void size  $d_i$  along each direction (Fig. 2) becomes a dependent design variable:

$$d_i = \frac{L_i}{2} - T$$

Consequently, different scale factors  $k_i$  lead to directional changes in the pore size, resulting in the structural anisotropy of the gyroid.

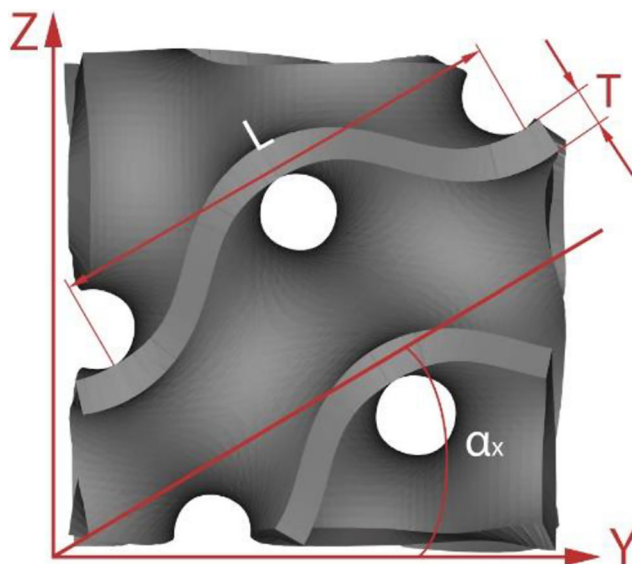


Fig. 1 Example of the elementary unit of a gyroid surface

On this basis, an experimental plan was designed (Table 1) and a synthetic label, including the values of the design parameters, was assigned to each gyroid  $G$ . Two values of wall thickness, namely, 0.4 and 0.6 mm, were tested in compliance with the resolution allowed by the building process, as discussed in the corresponding section. Different orientations  $\alpha_x$  of the wave were also considered. In the case of equal wavelengths along each axis, sweeping the orientation in the range 0–45° implies a complete investigation, assuming symmetry in a 45° direction (e.g. 80° orientation is equivalent to 10°). Note that the symmetry is lost when different scale factors  $k_i$  are applied along the axes.

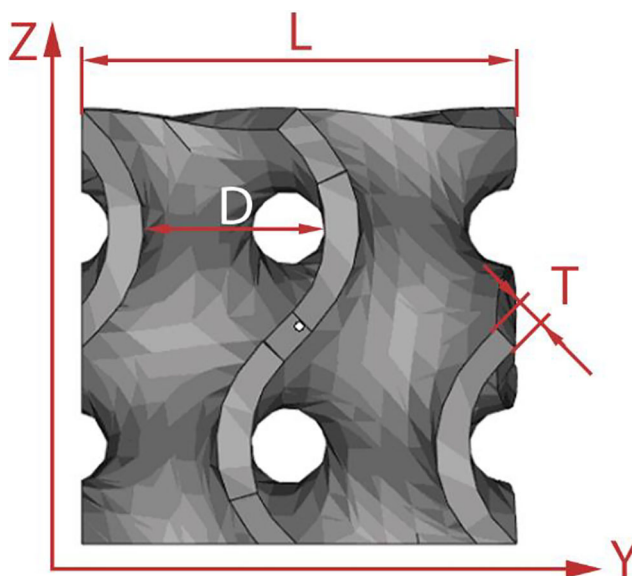
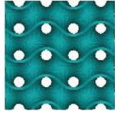
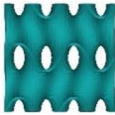
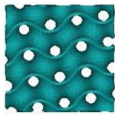
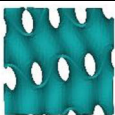
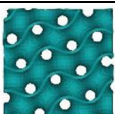
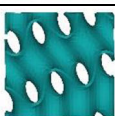
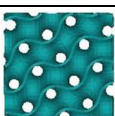
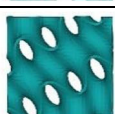
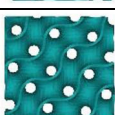
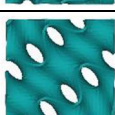
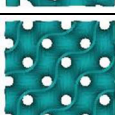
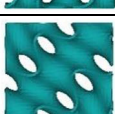


Fig. 2 Definition of the void size along a given direction

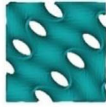
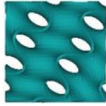
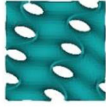
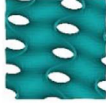
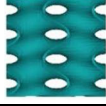
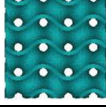
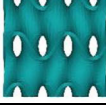
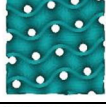

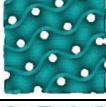
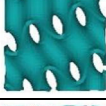
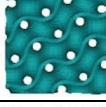
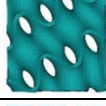
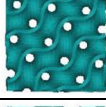

**Table 1** Design parameters, labels and nominal structure of the gyroids in the experimental plan

$T$ [mm]	$\alpha_x$ [°]	$k_x$	$k_y$	$k_z$	Label	Nominal structure
0.4	0	1	1	1	G/0.4/00/1-1-1	
		1	1	2	G/0.4/00/1-1-2	
	10	1	1	1	G/0.4/10/1-1-1	
		1	1	2	G/0.4/10/1-1-2	
	20	1	1	1	G/0.4/20/1-1-1	
		1	1	2	G/0.4/20/1-1-2	
	30	1	1	1	G/0.4/30/1-1-1	
		1	1	2	G/0.4/30/1-1-2	
	40	1	1	1	G/0.4/40/1-1-1	
		1	1	2	G/0.4/40/1-1-2	
	45	1	1	1	G/0.4/45/1-1-1	
		1	1	2	G/0.4/45/1-1-2	

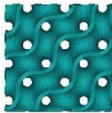
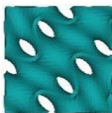
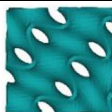
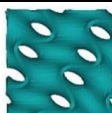
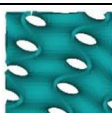
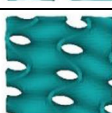
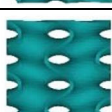
The scale factor was varied along the  $z$ -axis alone. A reference wavelength  $L$  of 7.5 mm was selected, thus providing a representative arrangement of elementary

units within a  $30 \times 30 \times 30$  mm domain. This choice was driven by the need for a constant theoretical void fraction for each given wall thickness and combination

Table 1 (continued)

	50	1	1	2	G/0.4/50/1-1-2	
	60	1	1	2	G/0.4/60/1-1-2	
	70	1	1	2	G/0.4/70/1-1-2	
	80	1	1	2	G/0.4/80/1-1-2	
	90	1	1	2	G/0.4/90/1-1-2	
0.6	0	1	1	1	G/0.6/00/1-1-1	
		1	1	2	G/0.6/00/1-1-2	
	10	1	1	1	G/0.6/10/1-1-1	
		1	1	2	G/0.6/10/1-1-2	
	20	1	1	1	G/0.6/20/1-1-1	
		1	1	2	G/0.6/20/1-1-2	
	30	1	1	1	G/0.6/30/1-1-1	
		1	1	2	G/0.6/30/1-1-2	
	40	1	1	1	G/0.6/40/1-1-1	
		1	1	2	G/0.6/40/1-1-2	

**Table 1** (continued)

	45	1	1	1	G/0.6/45/1-1-1	
		1	1	2	G/0.6/45/1-1-2	
	50	1	1	2	G/0.6/50/1-1-2	
	60	1	1	2	G/0.6/60/1-1-2	
	70	1	1	2	G/0.6/70/1-1-2	
	80	1	1	2	G/0.6/80/1-1-2	
	90	1	1	2	G/0.6/90/1-1-2	

of scale factors, irrespective of the  $\alpha$  orientation (Table 2).

The 3D surfaces representing the gyroids were conceived in Matlab, which allowed a modelling accuracy of 0.1 mm. Concerning the wall thickness  $T$ , it was set via software Blender. Eventually, the resulting .stl file was fixed via the Materialise Magics software prior to manufacturing to prevent common errors in terms of shapes and inverted normal and bad edges [41]. These errors are common in file conversions and even more frequent in case of lattice structures with consistent void fraction [42].

### 2.2 Manufacturing

Argon-atomised and pre-alloyed stainless steel powder was used to manufacture the gyroids. The mean grain size of the powder was 36  $\mu\text{m}$ . The composition matched the standard UNS S17400 chromium-copper precipitation hardening steel, offering high strength and corrosion resistance for mechanical applications [43, 44], as well as biocompatibility for medical implants [45]. The powder was processed by means of laser powder-bed fusion using a commercial EOSINT M270 laser sintering system operating in full-melting mode.

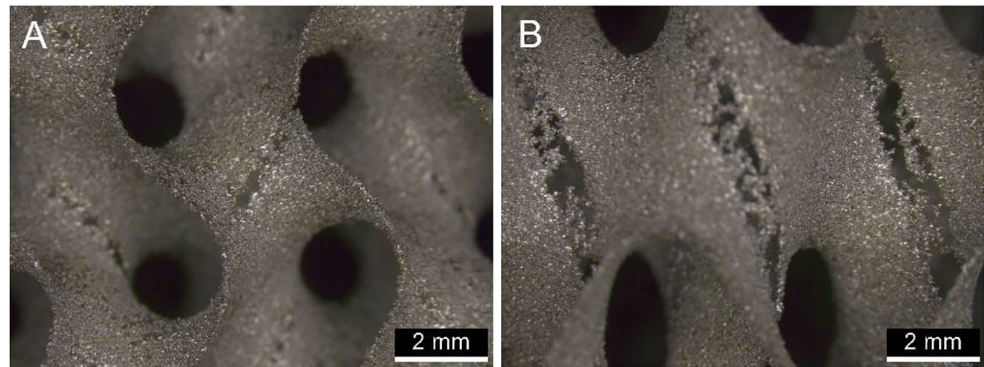
**Table 2** Theoretical void fraction

$T$ [mm]	$k_x$	$k_y$	$k_z$	Theoretical void fraction [%]
0.4	1	1	1	83.75
	1	1	2	85.95
0.6	1	1	1	75.80
	1	1	2	79.00

**Table 3** Values of the processing parameters in laser powder-bed fusion in full-melting mode

Parameter	Value
Laser power (W)	195
Scanning speed (m/s)	0.75
Hatch spacing ( $\mu\text{m}$ )	100
Scan length (mm)	20
Layer thickness ( $\mu\text{m}$ )	20

**Fig. 3** Example of manufacturing defects of 0.2-mm-thick walls in symmetric (A) and asymmetric (B) gyroids



The levels of the governing factors (Table 3) were set according to previous trials and tuning [41, 43, 46]. At the pre-design stage, the wall thicknesses of the gyroids in the experimental plan were set to 0.4 and 0.6 mm to comply with the resolution specified by the building process. It has been reported [41] that, depending on a number of factors (e.g. the AM system, the average grain size of the metal powder and the focusability of the laser beam), building thin walls below a given threshold is not feasible; otherwise collapse, defects and even job halts can occur. Although supporting structures offer a valid solution, they are not feasible in the case of TPMSs with interconnected voids. As an example, macroscopic defects resulting from a 0.2-mm wall thickness are depicted in Fig. 3.

### 2.3 Testing

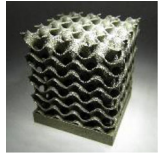
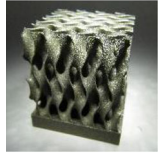
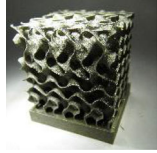
Preliminary inspections were conducted to verify the accuracy of the building process in terms of wall thickness. To this end, a Leica S8-APO stereo microscope with apochromatic  $\times 8$

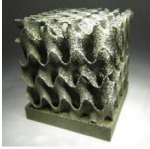

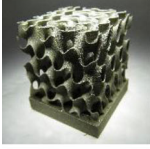


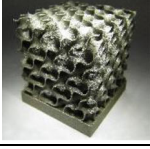


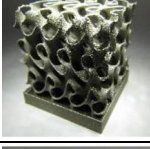


magnification and 75-mm working distance was used to measure the wall thickness at five random locations on each sample. Then, compressive strength tests were conducted on each gyroid in the experimental plan. For this, an MTS Landmark servo-hydraulic machine with a 250-kN force range and 3-Hz sampling rate was used. The testing method was performed under displacement control according to a prior study [19] on the testing of AM-made gyroid structures. The samples were tested up to 6% compressive deformation.

## 3 Results and discussion

Manufacturing was effectively accomplished for the gyroids in the experimental plan (Table 4). The actual wall thickness, the percentage mismatch as relative error with respect to the nominal thickness, the elastic modulus and the yield strength were measured, as discussed below.


**Table 4** Average wall thickness, percentage mismatch, Young modulus and yield strength of the gyroids in the experimental plan

Label	Actual structure (30 mm size cube)	Wall thickness [ $\mu\text{m}$ ]	Mismatch [%]	Elastic modulus [MPa]	Yield strength [MPa]
G/0.4/00/1-1-1		399.8	-0.1	602	15.4
G/0.4/00/1-1-2		409.8	2.4	1128	17.3
G/0.4/10/1-1-1		401.2	0.3	730	15.3

G/0.4/10/1-1-2		410.0	2.5	1328	20.5
G/0.4/20/1-1-1		413.2	4.1	962	15.8
G/0.4/20/1-1-2		406.0	1.5	1143	17.1
G/0.4/30/1-1-1		400.0	0.0	924	16.5
G/0.4/30/1-1-2		404.8	1.2	1055	14.3
G/0.4/40/1-1-1		398.6	-0.4	736	15.8
G/0.4/40/1-1-2		398.6	-0.4	825	11.4
G/0.4/45/1-1-1		399.6	-0.1	376	14.3
G/0.4/45/1-1-2		401.4	0.3	517	10.8
G/0.4/50/1-1-2		399.4	-0.2	683	9.4
G/0.4/60/1-1-2		395.2	-1.2	226	8.5



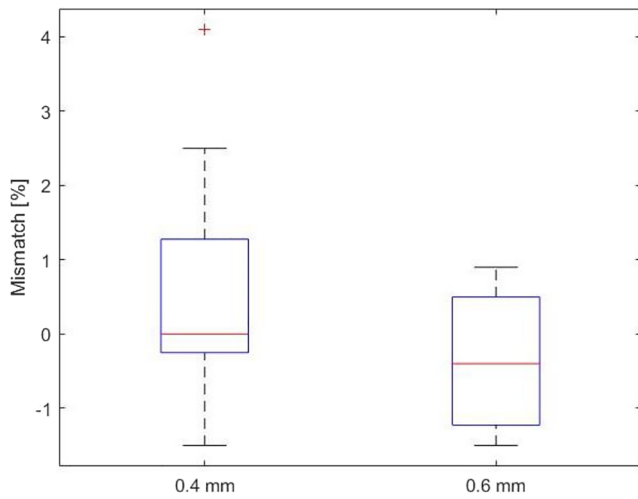
G/0.4/70/1-1-2		394.2	-1.5	367	7.8
G/0.4/80/1-1-2		401.2	0.3	384	7.3
G/0.4/90/1-1-2		399.2	-0.2	397	7.5
G/0.6/00/1-1-1		603.8	0.6	1346	28.5
G/0.6/00/1-1-2		591.0	-1.5	1699	40.6
G/0.6/10/1-1-1		602.8	0.5	1104	27.2
G/0.6/10/1-1-2		602.0	0.3	2149	37.5
G/0.6/20/1-1-1		605.0	0.8	1360	30.4
G/0.6/20/1-1-2		603.0	0.5	1729	37.3
G/0.6/30/1-1-1		597.2	-0.5	1041	30.8
G/0.6/30/1-1-2		597.8	-0.4	1786	28.4

G/0.6/40/1-1-1		603.2	0.5	1417	32.4
G/0.6/40/1-1-2		600.8	0.1	1469	26.0
G/0.6/45/1-1-1		605.4	0.9	1451	32.1
G/0.6/45/1-1-2		595.6	-0.7	1029	23.6
G/0.6/50/1-1-2		592.2	-1.3	634	22.5
G/0.6/60/1-1-2		591.0	-1.5	741	19.1
G/0.6/70/1-1-2		590.8	-1.5	604	17.5
G/0.6/80/1-1-2		595.4	-0.8	494	16.0
G/0.6/90/1-1-2		592.0	-1.2	460	16.5

### 3.1 Accuracy of the manufacturing process

The wall thickness at different random locations on each sample was measured via optical microscopy to assess the consistency and accuracy of the building process. Average errors of 0.5%

and 0.3% were found with respect to the nominal thicknesses of 0.4 and 0.6 mm, respectively. Reduced dispersion was achieved for increased nominal wall thickness (Fig. 4). Therefore, in terms of manufacturability, higher precision is inferred, in comparison to similar works in the literature [19, 38].

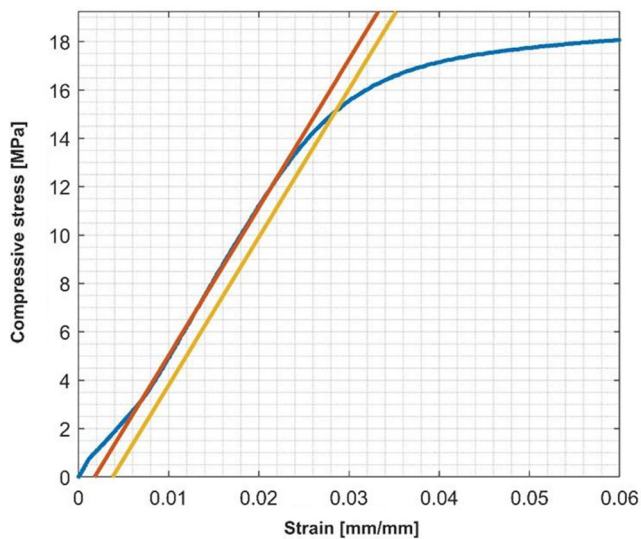


**Fig. 4** Box and whisker plot for percentage mismatch with respect to the nominal wall thickness

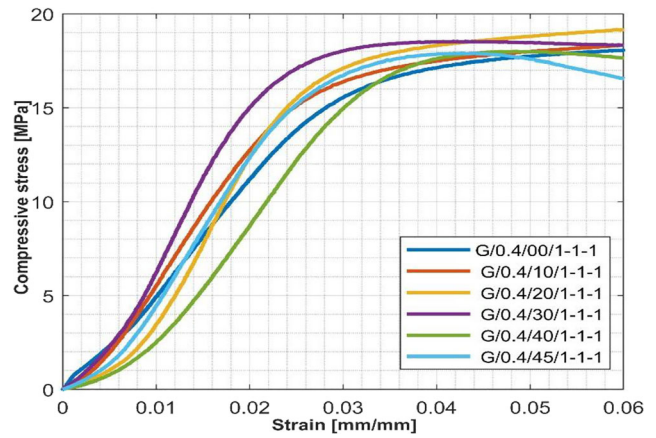
### 3.2 Mechanical properties

The trend of the stress-strain diagram is descriptive of the failure mode. In general (Fig. 5), a nonlinear stage was found at test initiation, before the typical linear elastic stage, due to settlement of the samples, until a condition of full contact between the crosshead of the testing machine and the surface of the gyroid was reached. This behaviour is typical in the testing of porous scaffold structures and has been already reported in the literature [19, 47]. Moreover, given that yielding is not evident, the yield strength was evaluated at a 0.2% strain offset with respect to the elastic stage.

The trend of the stress-strain curve clearly depends on the design parameters: when 1-1-1-type gyroids were considered (Figs. 6 and 7), a layer collapse occurred at higher deformation



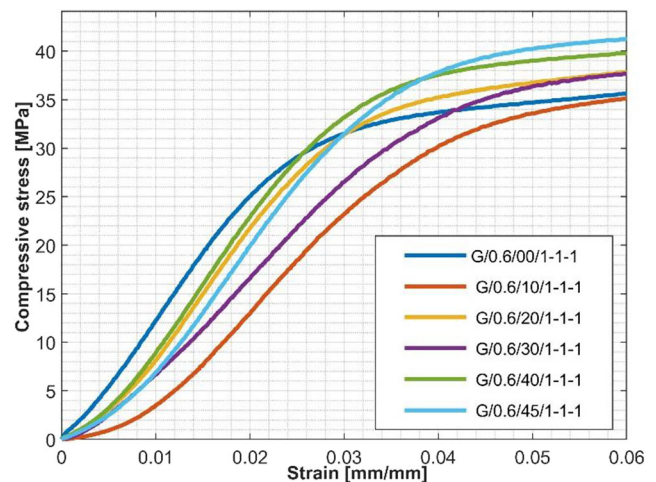
**Fig. 5** Stress-strain curve and determination of yield stress for a G/0.4/00/1-1-1 gyroid



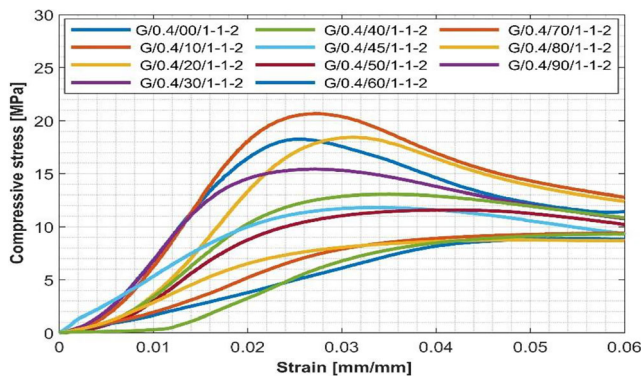
**Fig. 6** Stress-strain curves: gyroids of 1-1-1 type with 0.4-mm wall thickness

due to a reduced void fraction with respect to 1-1-2 type gyroids (Figs. 8 and 9). Nevertheless, 1-1-2-type gyroids improved the overall mechanical performance in terms of both elastic modulus and yield strength owing to a non-uniform geometry of voids that is beneficial for accommodating mechanical deformation and shear stresses.

To discuss the mechanical behaviour further, the elastic modulus and yield strength can be conveniently expressed as a function of thickness and orientation for each given class of gyroids. First, for the 1-1-1-type gyroids, orientation barely affected the mechanical response (Figs. 10 and 11). Any apparent dependence could be ascribed to a combination of possible inner local defects of incomplete fusion and reduced wall thickness due to manufacturing inaccuracy in the case of 0.4 mm, as previously mentioned. As expected, increased wall thickness resulted in increased modulus and strength, with average



**Fig. 7** Stress-strain curves: gyroids of 1-1-1 type with 0.6-mm wall thickness



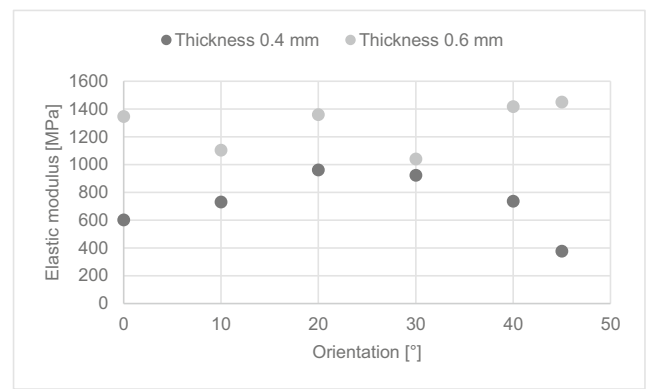
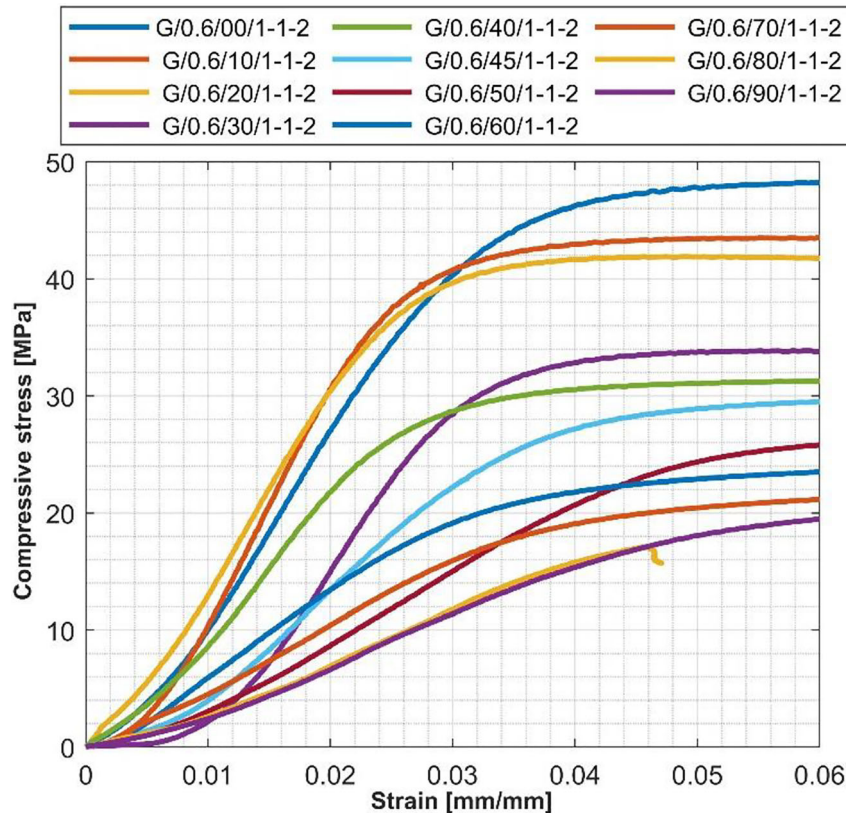
**Fig. 8** Stress-strain curves: gyroids of 1-1-2 type with 0.4-mm wall thickness

measurements of 78% and 95%, respectively. The behaviour in the range of 45–90° orientation can be inferred from symmetry through axis permutation, as discussed in the pre-design stage.

Concerning the 1-1-2-type gyroids, the effect of orientation over the mechanical response was significant (Figs. 12 and 13) and a linear predicting model (Table 5) could be derived for the mechanical response  $y$ , which expresses the elastic modulus or the yield strength in megapascals, as a function of orientation  $\alpha$  in degrees:

$$y = c_1 - c_2\alpha$$

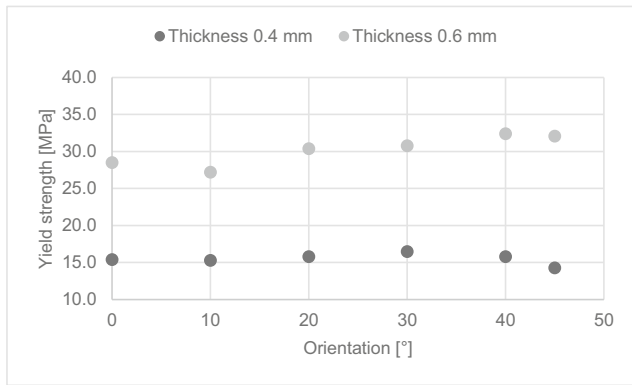
**Fig. 9** Stress-strain curves: gyroids of 1-1-2 type with 0.6-mm wall thickness



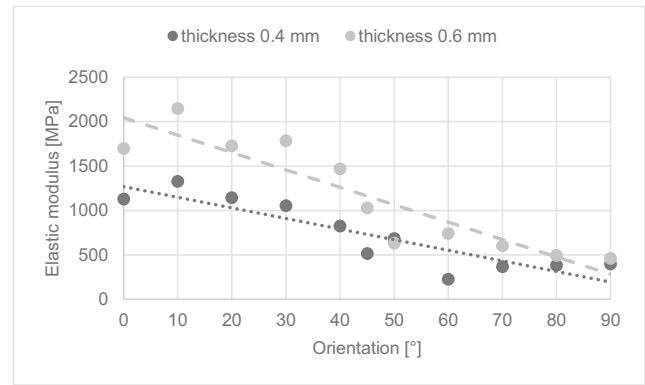
**Fig. 10** Elastic modulus as a function of wall thickness and orientation for 1-1-1-type gyroids

Note that rotating the direction of arrangement of the elementary units resulted in reduced elastic modulus and yield strength: this mechanical behaviour is equivalent to coil spring compression (Fig. 14); therefore, the equivalent wire windings resulting from the orientation angle is a factor. Again, a 50% increase in wall thickness resulted in increased modulus and strength, with average measurements of 60% and 115%, respectively.

We must conclude this section with a final crucial remark regarding the effect of the surface texture, which is a factor affecting the mechanical properties in the



**Fig. 11** Yield strength as a function of wall thickness and orientation for 1-1-1-type gyroids



**Fig. 12** Elastic modulus as a function of wall thickness and orientation for 1-1-2-type gyroids

AM of metals. Given that as-built arithmetic roughness in powder-bed fusion in full-melting mode typically ranges from 6 to 17  $\mu\text{m}$  [48], depending on the building direction, a significant variation in the surface features is expected within each given scaffold. Owing to the complex shape of the cells, post-processing to reduce the surface roughness is feasible with neither conventional nor innovative methods. However, a BTE-oriented application is not compromised: indeed, surface roughness is expected to be beneficial in promoting tissue regeneration.

The range of mechanical features of the trabecular bone of tibias and vertebrae are successfully achieved [2, 3] by the gyroids in this experimental plan. Convenient orientations, wall thickness values and wavelength elongations can be further investigated to extend the applications to other bones.

### 4 Conclusions

At present, the accuracy of AM technology is still a factor hindering some potential applications of gyroids. Although the manufacturability depends on the available powder and machine, the adoption of a wall thickness below a technical

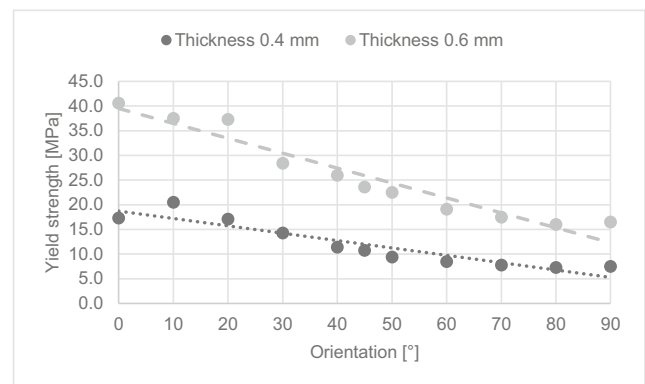
threshold of 0.2 mm has not been feasible using full-melting mode in laser powder-bed fusion.

Nevertheless, it has been proved in this study that a convenient setting of the geometric parameters of a gyroid structure, such as orientation and wavelength, is effective in allowing the designer to properly manage a wide variety of cases, matching the required mechanical properties of the trabecular bone for tibias and vertebrae. The following main findings of our study can be highlighted:

- There is no need for supporting structures during fabrication of gyroids in the full-melting mode via laser powder-bed fusion.
- Suitable accuracy of the wall thickness is achieved with a percentage mismatch in the order of 0.5 and 0.3% for nominal thickness of 0.4 and 0.6 mm, respectively.
- Orientation barely affects the mechanical response when the same scale factor is applied along each axis of the gyroid.

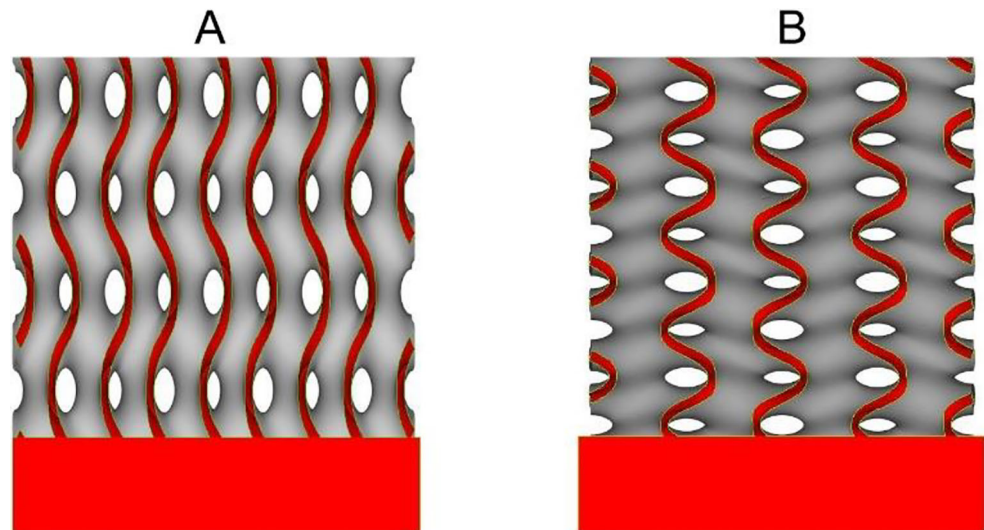
**Table 5** Calibration constants and correlation coefficient for each response for 1-1-2-type gyroids

Response (MPa)	Wall thickness (mm)	$c_1$	$c_2$	Model $R^2$
Elastic modulus	0.4	1270	11.9	0.80
	0.6	2045	19.6	0.83
Yield strength	0.4	18.7	0.15	0.87
	0.6	39.5	0.30	0.93



**Fig. 13** Yield strength as a function of wall thickness and orientation for 1-1-2-type gyroids

**Fig. 14** Coil spring compression analogy for 0.6-mm 1-1-2-type gyroids with 0° orientation (A) and 90° orientation (B)



- When a scale factor is applied along one of the axes of the gyroid, the mechanical behaviour is equivalent to coil spring compression; therefore, both the elastic modulus and yield strength decrease with increasing orientation of the arrangement of the elementary units.

Further tests must be conducted to investigate the fatigue behaviour of the gyroids; in addition, a simulation approach must be implemented to find the response on a case-by-case basis and reduce the need for new wide experimental trials.

**Code availability** Data required to reproduce the code are given in the text. If needed, they can be shared upon request.

**Funding** Open access funding provided by Università degli Studi di Salerno within the CRUI-CARE Agreement. This work was supported by the University of Salerno through the project “Additive Manufacturing and Mechanical Testing of Gyroids for Human Bones”.

**Data availability** Data required to reproduce these findings have been given in the text. Any additional data can be shared upon request.

## Declarations

**Ethical approval** This material is the authors’ own original work, which has not been previously published elsewhere.

**Competing interests** There is no competing of interest within this paper.

**Open Access** This article is licensed under a Creative Commons Attribution 4.0 International License, which permits use, sharing, adaptation, distribution and reproduction in any medium or format, as long as you give appropriate credit to the original author(s) and the source, provide a link to the Creative Commons licence, and indicate if changes were made. The images or other third party material in this article are included in the article’s Creative Commons licence, unless indicated otherwise in a credit line to the material. If material is not included in the article’s Creative Commons licence and your intended use is not permitted by

statutory regulation or exceeds the permitted use, you will need to obtain permission directly from the copyright holder. To view a copy of this licence, visit <http://creativecommons.org/licenses/by/4.0/>.

## References

1. Deb P, Barua E, Deoghare A, Das Lala S (2019) Development of bone scaffold using *Puntius conchoniuis* fish scale derived hydroxyapatite: psycho-mechanical and bioactivity evaluations. *Ceram Int* 45:10004–10012
2. Wu D, Isaksson P, Ferguson S, Persson C (2018) Young’s modulus of trabecular bone at the tissue level: a review. *Acta Biomater* 78:1–12
3. Keaveny T, Morgan E, Niebur G, Yen C (2001) Biomechanics of trabecular bone. *Annu Rev Biomed Eng* 3:307–333
4. Yang L, Yan C, Fan H, Li Z, Cai C, Chen P, Shi Y, Yang S (2019) Investigation on the orientation dependence of elastic response in gyroid cellular structures. *J Mech Behav Biomed Mater* 90:73–85
5. Amini A, Laurencin C, Nukavarapu S (2012) Bone tissue engineering: recent advances and challenges. *Crit Rev Biomed Eng* 40(5): 363–408
6. Chocholata P, Kulda V, Babuska V (2019) Fabrication of scaffolds for bone-tissue regeneration. *Materials* 12(4):568
7. Hutmacher D (2000) Scaffolds in tissue engineering bone and cartilage. *Biomaterials* 21:2529–2543
8. Jain R, Au P, Tam J, Duda D, Fukumura D (2005) Engineering vascularized tissue. *Nat Biotechnol* 23:821–823
9. Bose S, Roy M, Bandyopadhyay A (2012) Recent advances in bone tissue engineering scaffolds. *Trends Biotechnol* 30(10):546–552
10. Giannitelli S, Accoto D, Trombetta M, Rainer A (2014) Current trends in the design of scaffolds for computer-aided tissue engineering. *Acta Biomater* 10:580–594
11. Ghayor C, Weber F (2018) Osteoconductive microarchitecture of bone substitutes for bone regeneration revisited. *Front Physiol* 9:1–8
12. Kumar A, Nune K, Murr L, Misra R (2016) Biocompatibility and mechanical behaviour of three-dimensional scaffolds for biomedical devices: process-structure-property paradigm. *Int Mater Rev* 61(1):20–45
13. Khoda A, Ozbolat I, Koc B (2013) Designing heterogeneous porous tissue scaffolds for additive manufacturing processes. *Comput Aided Des* 45(12):1507–1523

14. Aslan B, Yildiz A (2020) Optimum design of automobile components using lattice structures for additive manufacturing. *Mater Test* 62(6):633–639
15. Caiazzo F, Alfieri V, Corrado G, Argenio P (2017) Laser powderbed fusion of Inconel 718 to manufacture turbine blades. *Int J Adv Manuf Technol* 93(9–12):4023–4031
16. Uriondo E-MP (2015) The present and future of additive manufacturing in the aerospace sector: a review of important aspects. *J Aerosp Eng* 229(11):2132–2147
17. Rosen D (2007) Computer-aided design for additive manufacturing of cellular structures. *Comput Aided Des Appl* 4(5):585–594
18. Singh S, Ramakrishna S, Singh R (2017) Material issues in additive manufacturing: a review. *J Manuf Process* (25):182–200
19. Ma S, Tang Q, Feng Q, Song J, Han X, Guo F (2019) Mechanical behaviours and mass transport properties of bone-mimicking scaffolds of gyroid structures manufactured using selective laser melting. *J Mech Behav Biomed Mater* 93:158–169
20. Bobbert F, Lietaert K, Eftekhari A, Pouran B, Ahmadi S, Weinans H, Zadpoor A (2017) Additively manufactured metallic porous biomaterials based on minimal surfaces: a unique combination of topological, mechanical and mass transport properties. *Acta Biomater* 53:572–584
21. Yanez A, Herrera A, Martel O, Monopoli D, Afonso H (2016) Compressive behaviour of gyroid lattice structures for human cancellous bone implant applications. *Mater Sci Eng C* 68:445–448
22. Ataee A, Yuncang L, Fraser D, Song G, Wen C (2018) Anisotropic Ti-6Al-4 V gyroid scaffolds manufactured by electron beam melting (EBM) for bone implant applications. *Mater Des* 137:345–354
23. Tan X, Tan Y, Chow C, Tor S, Yeong W (2017) Metallic powderbed based 3D printing of cellular scaffolds for orthopaedic implants: a state-of-the-art review on manufacturing, topological design, mechanical properties and biocompatibility. *Mater Sci Eng C* 76:1328–1343
24. Mahmoud D, Al-Rubaie K, Elbestawi M (2021) The influence of selective laser melting defects on the fatigue properties of Ti6Al4V porosity graded gyroids for bone implants. *Int J Mech Sci* 193
25. Mahmoud D, Elbestawi M (2019) Selective laser melting of porosity graded lattice structures for bone implants. *Int J Adv Manuf Technol* 100:2915–2927
26. Caiazzo F, Alfieri V, Casalino G (2020) On the relevance of volumetric energy density in the investigation of Inconel 718 laser powder bed fusion. *Materials* 13:538–549
27. Cesarano J, Dellinger J, Saavedra M, Gill D (2005) Customization of load-bearing hydroxyapatite lattice scaffolds. *Int J Appl Ceram Technol* 2(3):212–220
28. Cheah C, Chua C, Leong K, Cheong CH, Naing M (2004) Automatic algorithm for generating complex polyhedral. *Tissue Eng* 10:595–610
29. Yang E, Leary M, Lozanovski B, Downing D, Mazur M, Sarker A, Khorasani A, Jones A, Maconachie T, Bateman S, Easton M, Qian M, Choong P, Brandt M (2019) Effect of geometry on the mechanical properties of Ti-6Al-4 V gyroid structures fabricated via SLM: a numerical study. *Mater Des* 184:1–24
30. Jinnai H, Watashiba H, Kajihara T, Nishikawa Y, Takahashi M, Ito M (2002) Surface curvatures of trabecular bone microarchitecture. *Bone* 30(1):191–194
31. Hao L, Raymond D, Yan C, Hussein A, Young P (2012) Design and additive manufacturing of cellular lattice structures. In: *Innovative developments in virtual and physical prototyping*. CRC Press, pp 249–254
32. Hollister S (2005) Porous scaffold design for tissue engineering. *Nat Mater* 4:518–524
33. Yan C, Hao L, Hussein A, Young P (2015) Ti-6Al-4 V triply periodic minimal surface structures for bone implants fabricated via selective laser melting. *J Mech Behav Biomed Mater* 51:61–73
34. Olivares A, Marshal E, Planell J, Lacroix D (2009) Finite element study of scaffold architecture design and culture conditions for tissue engineering. *Biomaterials* 30:6142–6149
35. Jung G, Buehler M (2018) Multiscale mechanics of triply periodic minimal surfaces of three-dimensional graphene foams. *Nano Lett* 18(8):4845–4853
36. Feng Q, Tang Q, Liu Y, Setchi R, Soe S, Ma S, Bai L (2017) Quasi-static analysis of mechanical properties of Ti6Al4V lattice structures manufactured using selective laser melting. *Int J Adv Manuf Technol*:1–13
37. Yang Y, Wang G, Liang H, Gao C, Peng S, Shen L, Shuai C (2019) Additive manufacturing of bone scaffolds. *Int J Bioprint* 5(1)
38. Maszybrocka J, Gapiński B, Dworak M, Skrabalak G, Stwora A (2019) The manufacturability and compression properties of the Schwarz diamond type Ti6Al4V cellular lattice fabricated by selective laser melting. *Int J Adv Manuf Technol* 105:3411–3425
39. Mahmoud D, Elbestawi M, Yu B (2019) Process–structure–property relationships in selective laser melting of porosity graded gyroids. *J Med Dev* 13(3):1–11
40. Speirs M, Van Hooreweder B, Van Humbeeck J, Kruth J (2017) Fatigue behaviour of NiTi shape memory alloy scaffolds produced by SLM, a unit cell design comparison. *J Mech Behav Biomed Mater* 70:53–59
41. Contuzzi N, Campanelli S, Caiazzo F, Alfieri V (2019) Design and fabrication of random metal foam structures for laser powder bed fusion. *Materials* 12(1301):1–13
42. Chougrani L, Pernot J, Véron P, Abed S (2017) Lattice structure lightweight triangulation for additive manufacturing. *Comput Aided Des* 90:95–104
43. Usera D, Alfieri V, Caiazzo F, Argenio P, Corrado G, Ares E (2017) Redesign and manufacturing of a metal towing hook via laser additive manufacturing with powder bed. *Procedia Manuf* (13):825–832
44. Riazi H, Ashrafizadeh F, Hosseini S, Ghomashchi R, Liu R (2017) Characterization of simultaneous aged and plasma nitrided 17-4 PH stainless steel. *Mater Charact* 133:33–43
45. Pradeep PremKumar K, Duraipandy N (2018) Antibacterial effects, biocompatibility and electrochemical behavior of zinc incorporated niobium oxide coating on 316 L SS for biomedical applications. *Appl Surf Sci B* 427:1166–1181
46. Cardaropoli F, Alfieri V, Caiazzo F, Sergi V (2012) Dimensional analysis for the definition of the influence of process parameters in selective laser melting of Ti-6Al-4 V alloy. *J Eng Manuf* 7(226):1136–1142
47. Feng Q, Tang Q, Liu Y, Setchi R, Soe S, Ma S, Bai L (2018) Quasi-static analysis of mechanical properties of Ti6Al4V lattice structures manufactured using selective laser melting. *Int J Adv Manuf Technol* 94(5–8):2301–2313
48. Alfieri V, Argenio P, Caiazzo F, Sergi V (2017) Reduction of surface roughness by means of laser processing over additive manufacturing metal parts. *Materials* 10(30):1–12